Materials Science and Engineering C 41 (2014) 161–167

Contents lists available at ScienceDirect

Materials Science and Engineering C

journal homepage: www.elsevier.com/locate/msec

One-pot facile synthesis of PEGylated superparamagnetic iron oxide nanoparticles for MRI contrast enhancement

Lingling Dai [a], Yongkang Liu [a], Zhongqiu Wang [a,*], Fangfang Guo [b], Donglu Shi [b,c], Bingbo Zhang [b,*]

[a] Department of Radiology, Affiliated Hospital of Nanjing University of Traditional Chinese Medicine (TCM), Nanjing 210029 Jiangsu, China
[b] Shanghai East Hospital, The Institute for Biomedical Engineering & Nano Science, Tongji University School of Medicine, Shanghai 200120, China
[c] Materials Science and Engineering Program, Dept. of Mechanical and Materials Engineering, College of Engineering and Applied Science, University of Cincinnati, Cincinnati, OH 45221, USA

ARTICLE INFO

Article history:
Received 4 December 2013
Received in revised form 12 April 2014
Accepted 18 April 2014
Available online 28 April 2014

Keywords:
Superparamagnetic iron oxide
Polyethylene glycol
Magnetic resonance imaging
Biomedical imaging
Contrast agent

ABSTRACT

Polyethylene glycol (PEG)-coated superparamagnetic iron oxide nanoparticles (PEG·SPIONs) were prepared by a facile one-pot approach. The synthesized PEG·SPIONs were found to be uniform in size with an average hydrodynamic diameter of 11.7 nm. PEG·SPIONs exhibited excellent dispersibility in water, colloidal stability, and biocompatibility. The magnetic resonance imaging (MRI) properties of PEG·SPIONs were characterized both *in vitro* and *in vivo*. The dual contrast both in T_1 and T_2-weighted imaging was well enhanced with longitudinal and transverse relaxivity (r_1, r_2) of 35.92 s^{-1} per mM of Fe^{3+} and 206.91 s^{-1} per mM of Fe^{3+} respectively. *In vivo* T_2-weighted MRI shows pronounced enhancement in the liver and spleen but not in T_1-weighted MRI. Accumulations of nanoparticles were found primarily in the liver, spleen, and intestine, while much lower uptake in the kidney, heart, and lungs. A gradual excretion of PEG·SPIONs was observed *via* hepatobiliary (HB) processing over a period of 14 days. The toxicity of PEG·SPIONs was also evaluated *in vitro* and *in vivo*. PEG·SPIONs were found to be biocompatible by investigating organ tissues after hematoxylin–eosin staining. The conclusion of the study indicates a high potential of PEG·SPIONs in medical MRI.

1. Introduction

Contrast-enhanced MRI is among the best clinical noninvasive methodologies known today for the assessment of anatomy and tissue functions [1–4]. Gd-DTPA, a frequently used contrast agent in clinics, can be rapidly cleared out by renal excretion with short residency time in organs such as the liver [5]. Furthermore, Gd-DTPA has been reported to be considerably toxic that is particularly harmful to the kidneys [6]. There is, therefore, a great need to search for biocompatible MRI contrast agents with a large imaging time-window and gradual excretion.

Compared to Gd-based contrast agents, superparamagnetic iron oxide nanoparticles (SPIONs) have been extensively investigated due to their unique magnetic properties and biocompatibility and considered a preferred alternative candidate for MRI [7,8]. SPIONs can be effectively taken up by macrophages in the liver with proper retention time, and then excreted gradually *via* hepatobiliary (HB) processing [9]. Feridex® and Revosit® were typical commercially available SPIONs, but terminated on the market in 2009 [10]. Extensive efforts have been devoted to the development of novel SPIONs in the last decade by both research groups and bio-pharmaceutical companies [11–13]. Most of the reported SPIONs are over 20 nm in sizes, and their required surface functionalization procedures are tedious. Among most of the surface functionalization, the capping ligands mainly include silica [14], dextran derivative [15], chitosan derivative [16], Poly-L-lysine [17,18], and poly (ethyleneimine) [19]. An alternative, more straight forward facile approach is needed for the ultra small biocompatible SPIONs (<20 nm).

Two most extensively used methods in preparing SPIONs for MRI are coprecipitation and thermal decomposition. The coprecipitation technique is probably the simplest chemical route in the preparation of SPIONs. But this method does not provide good control on size distribution and particle geometry [20]. In contrast, the thermal decomposition can produce a narrow size distribution [21]. Recently, the thermal decomposition of $Fe(acac)_3$ in high boiling alcohol solvent, such as PEG, poly(ethylene imine) (PEI) and poly(vinyl pyrrolidone) (PVP), is reported produce water soluble SPIONs [22]. Hu et al. also reported a facile synthesis of water-soluble, ultrasmall, PEGylated $Mn_xFe_{3-x}O_4$ nanoparticles for MRI application [23]. It combines the advantages of precipitation and thermal decomposition with hydrophilic nature for the control of size and geometry. And PEG coating can decorate nanoparticles with biocompatibility, hydrophilicity, soft surface, antifouling and long circulation *in vivo* [24,25] However, the *in vivo* imaging utilizing the SPIONs is yet to be investigated.

* Corresponding authors. Tel.: +86 21 65988029; fax: +86 21 65983706 0.
E-mail addresses: zhq2001us@163.com (Z. Wang), bingbozhang@tongji.edu.cn (B. Zhang).

http://dx.doi.org/10.1016/j.msec.2014.04.041
0928-4931/

In this study, a facile one-pot synthesis route is developed for the preparation of PEG·SPIONs. PEG·SPIONs are found to exhibit small hydrodynamic diameters and colloidal stability in a wide range of pH values and high ion strength. These PEG·SPIONs show pronounced MRI enhancement without adverse drug reactions *in vitro* and *in vivo*. They can also be gradually cleared *via* HB processing.

2. Materials and methods

2.1. Materials

All materials were used as received. $Fe(acac)_3$, poly(ethylene glycol) bis(carboxymethyl) ether (HOOC–PEG–COOH, 600 g/mol), tetraethylene glycol (TEG) were purchased from Sigma-Aldrich. Deionized water (18.2 M Ω · cm resistivity at 25 °C) was used in all experiments. The animal procedures complied with the guidelines of the Institutional Animal Care and Use Committee of Tongji University.

2.2. PEG·SPIONs synthesis

PEG·SPIONs were synthesized with minor modifications according to a previously published procedure [26]. Briefly, 2 mmol of $Fe(acac)_3$, 6 g of HOOC–PEG–COOH and 25 mL of TEG were mixed and purged with nitrogen for 30 min. The reaction mixture was magnetically stirred at 100 °C until all of the reagents were completely dissolved into the solvent. The mixture was heated to 210 °C for 2 h and then refluxed (ca. 287 °C) for another hour. After cooling to room temperature, the PEG·SPIONs were dialyzed against sodium citrate (0.2 M, pH 6.5) at room temperature for 24 h, and then washed with ethanol three times, and vacuum dried at room temperature. The purified PEG·SPIONs were weighed and redispersed in borate buffer solution (50 mM, pH 8.2) for future studies. The iron concentration of each sample was determined by inductively coupled plasma atomic emission spectroscopy (ICP-AES).

2.3. PEG·SPIONs characterization

The morphology and sizes of PEG·SPIONs were studied using a transmission electron microscope (TEM, Philips Tecnai G^2 F20) at an accelerating voltage of 200 kV. The samples were prepared by placing a drop of dilute aqueous dispersions on the surface of copper grids and air-dried. Hydrodynamic diameters of PEG·SPIONs were measured using a dynamic light scattering (DLS) particle size analyzer (Nano ZS90, Malvern). X-ray diffraction (XRD) measurement of PEG·SPIONs was carried out on a powder sample using a DX-1000 diffractometer with CuKα radiation ($\lambda = 0.15406$ nm). The magnetic property was analyzed using a vibrating sample magnetometer (VSM; Lakeshore 7407, USA) at 27 °C. Fourier transform infrared spectroscopy (FTIR) analysis was obtained with a Tensor27 FTIR spectrometer by using attenuated total reflectance (ATR) mode (BRUKER, Tensor 27).

2.4. Colloidal stability study of PEG·SPIONs

PEG·SPIONs were dispersed in various pH buffer solutions (pH value varies from 3 to 11) and sodium chloride water solutions (concentration varies from 0.25 M to 2 M) for one week at room temperature. The hydrodynamic diameters of the samples in every solution were determined by DLS measurement.

2.5. In vitro relaxometry

Longitudinal and transverse relaxation times were measured using a 1.41 T minispec mq 60 NMR Analyzer (Bruker, Germany) at 37 °C. PEG·SPIONs with different Fe^{3+} concentrations from 0.06 to 0.24 mM were prepared for relaxation time measurements. Relaxivity values of r_1 and r_2 were calculated by fitting the $1/T_1$ and $1/T_2$ relaxation time (s^{-1}) *versus* Fe^{3+} concentration (mM) curves. The *in vitro* MR images were obtained using a 3T MR scanner (Intera 3T, Philips Medical Systems). T_1-weighted image was acquired using a T_1-weighted spin echo pulse sequence with TR = 500 ms, TE = 8 ms, FOV = 100 × 120 mm^2, data matrix = 240 × 208, and slice thickness = 3 mm. T_2-weighted image was taken using a T_2-weighted spin echo pulse sequence with TR = 1200 ms, TE = 100 ms, FOV = 100 × 120 mm^2, data matrix = 280 × 216, and slice thickness = 3 mm.

2.6. In vitro cytotoxicity evaluation

The *in vitro* cytotoxicity was assessed by the 3-(4, 5-dimethylthiazol-2-yl)-2, 5-diphenyl-tetrazolium bromide (MTT) assay. NIH-3T3 cells growing in log phase were seeded in 96-well cell-culture plates at 5000 cells per well and incubated for 24 h at 37 °C under 5% CO_2. Dulbecco's Modified Eagle Medium (DMEM) supplemented with 10% FBS solutions of PEG·SPIONs (100 μL/well) at various concentrations of Fe^{3+} was added to the wells of the treatment group. For the control group, only DMEM (100 μL/well) was added without PEG·SPIONs. After 24 h and 48 h of incubation at 37 °C, 20 μL of MTT solution (5 mg/mL) was added into each well following additional 4 h incubation. Subsequently, the precipitated formazan was dissolved in dimethylsulfoxide (DMSO, 150 μL/well) for 10 min. A Tecan Infinite M200 monochromator-based multifunction microplate reader was used to measure OD570 (A value) of each well with the background subtraction at 690 nm. The following formula was used to calculate the viability of cell growth: cell viability (%) = (mean of IA value of treatment group/mean of IA value of control) × 100.

2.7. In vivo MRI

All animal experiments were conducted following a protocol approved by the Institutional Animal Care and Use Committee of Tongji University. Animals were anesthetized by intraperitoneal injection of pentobarbital sodium. PEG·SPIONs were injected into Balb/c mice (mouse mass ≈ 100 g, n = 3) through the tail vein at a dosage of 2.5 mg Fe/kg of mouse body weight. Mouse MR *in vivo* imaging was performed on a 3T MR imaging system (Intera 3 T, Philips Medical Systems) using a mouse coil with the following parameters: T_1-weighted imaging: TR = 300 ms, TE = 20 ms, FOV = 60 mm × 60 mm, data matrix = 148 × 150, and slice thickness = 1 mm. T_2-weighted imaging: TR = 5000 ms, TE = 50 ms, FOV = 60 mm × 60 mm, data matrix = 200 × 200, and slice thickness = 1 mm.

2.8. In vivo biodistribution and histology analysis

Four-to five-week-old Kunming mice (25–30 g of body weight) were purchased from the Second Military Medical University (Shanghai, China). The animal procedures followed the guidelines of the Institutional Animal Care and Use Committee of Tongji University. The PEG·SPIONs were injected intravenously in Kunming mice (n = 3) at a dose of 2.5 mg (Fe)/kg body weight. Three mice without injection were used as the blank control. All mice were sacrificed after complete anesthesia. Major organs were removed from mice post-injected with PEG·SPIONs at different intervals. The removed organs were pulverized and treated with nitric acid. The organ/nitric acid solutions were heated at 90 °C for 8 h and then filtered for ICP analysis.

Tissue samples were harvested from mice injected with PEG·SPIONs 15 days post-injection and from those receiving no injections. The heart, liver, spleen, lung, kidney and intestine were removed and fixed in paraformaldehyde, embedded in paraffin, sectioned, and stained with hematoxylin and eosin. The histological sections were observed under an optical microscope.

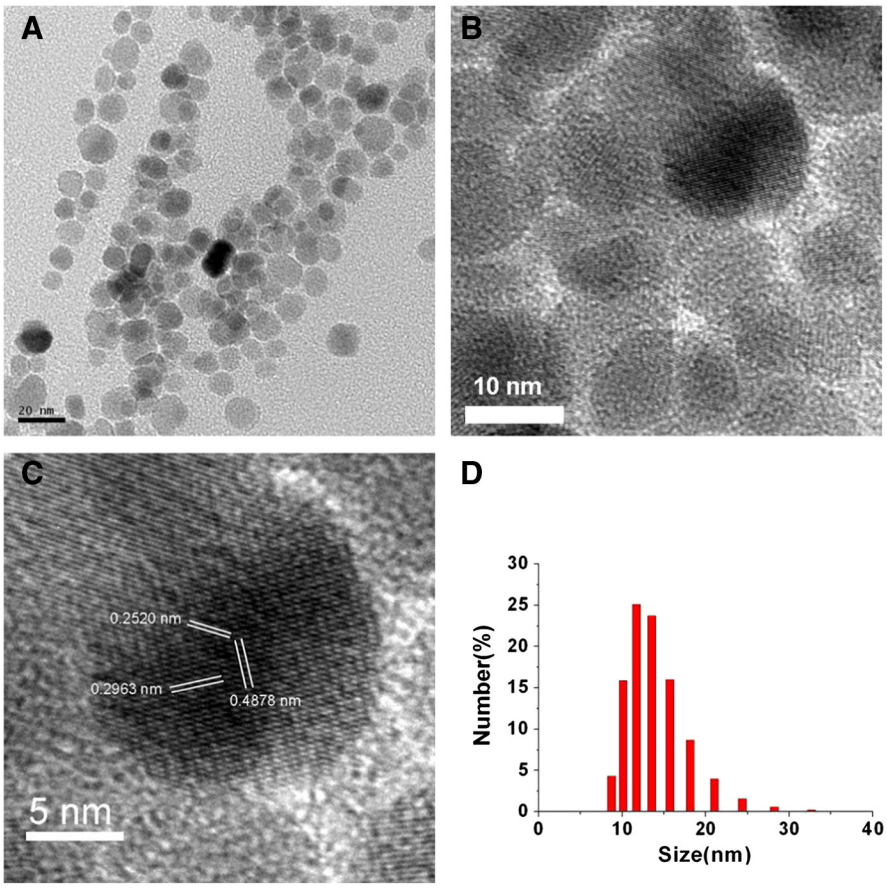

Fig. 1. TEM images (A, B, C) and DLS data (D) of PEG·SPIONs in water.

3. Results and discussion

3.1. Synthesis and characterization of PEG·SPIONs

In this study, a polyol process was developed to synthesize SPIONs. In this process, $Fe(acac)_3$ was used as the iron precursor, PEG as the stabilizer, and TEG as the solvent. Fig. 1A,B,C shows the representative TEM images of the PEG·SPIONs. From an overview TEM images, the as-prepared PEG·SPIONs are monodispersed in water without large aggregations. Fe_3O_4 nanoparticles synthesized in the oil phase by high temperature thermal decomposition are hydrophobic for their organic capping ligands anchored on particle surfaces. For biomedical applications, these nanoparticles must be surface modified for water dispersibility [27]. In this study, to effectively simplify the synthesis process, thermal decomposition was used in alcoholic solution with high boiling point. The as-prepared nanoparticles can be readily dispersible in water. The corresponding TEM characterization in Fig. 1C shows three kinds of the lattice fringes with lattice spacing of about 0.4878 nm, 02520 nm and 0.2963 nm corresponding to the {1 1 1}, {3 1 1} and {2 2 0} plane of Fe_3O_4. The hydrodynamic diameter of PEG·SPIONs in water is shown in Fig. 1D. The average hydrodynamic diameter is 11.7 nm. This size is relatively small compared to the previously reported [28]. The aggregation of Fe_3O_4 nanoparticles often occurs due to strong magnetic dipole–dipole interactions. Optimum synthesis relies on key parameters such as the polymer length or molecular weight, conformational arrangement on the

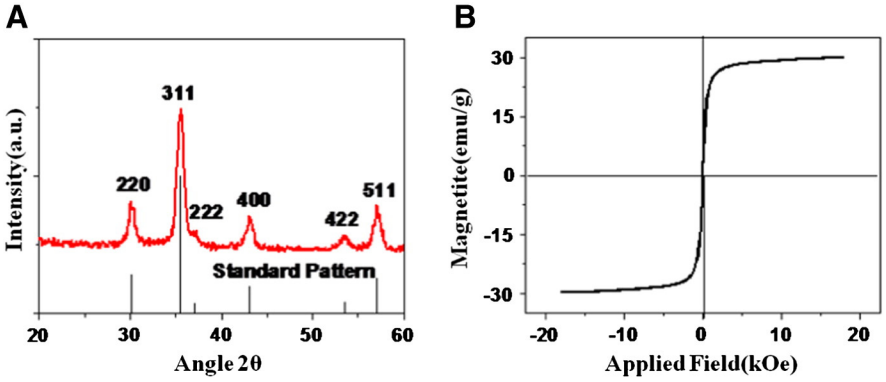

Fig. 2. XRD pattern (A) and magnetization curve (B) of PEG·SPIONs.

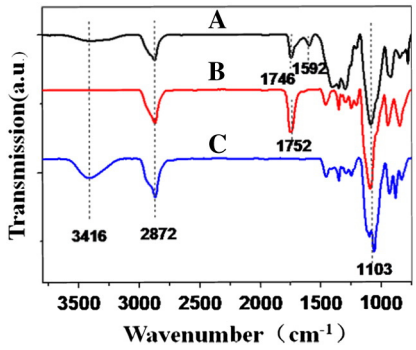

Fig. 3. FTIR spectra of PEG·SPIONs (A), COOH–PEG–COOH (B) and TEG (C).

surface, and surface coverage. These parameters dominate the nanoparticle stability in media such as biological buffers and cell cultures [29–31]. PEG has been widely used as a pharmacological product [32, 33]. Attachment of PEG chains to particle surfaces is known to promote water dispersibility, reduce toxicity, and decrease enzymatic degradation. As is also well known, the enhanced particle stability, based on PEG coating, can prolong their circulation half-life *in vivo* [34–36].

The XRD measurements were performed on the dried powders of PEG·SPIONs for phase analysis. As shown in Fig. 2A, the position and relative intensity of the strong diffraction peaks of PEG·SPIONs match well with typical XRD patterns of Fe_3O_4 (Joint committee on Powder Diffraction Standards, JCPDS 11-0614). High reaction temperature favors crystallinity and monodispersity of the nanoparticles, as evident in Figs. 1 and 2. Superparamagnetism is an essential property required for MRI. As is shown in Fig. 2B, the saturation magnetization of the PEG·SPIONs is 29.9 $emug^{-1}$ without remanent magnetization. This result indicates the superparamagnetic nature of PEG·SPIONs.

The surface chemical structure of PEG·SPIONs was characterized by Fourier transform infrared (FTIR) spectroscopy (Fig. 3). The distinct spectral difference between HOOC–PEG–COOH and the PEG·SPIONs is the carboxyl band at 1752 cm^{-1} for HOOC–PEG–COOH, being shifted to a lower wavenumber, 1746 cm^{-1}, accompanied by a new band at 1592 cm^{-1}. This shift could be a result of interaction between the carboxylate group and the surface iron of SPION [37]. A broad –O–H stretch around 3416 cm^{-1}, a sharp $-CH_2$ stretch around 2872 cm^{-1}, and a sharp –C–O–C stretch around 1103 cm^{-1} are observed in both PEG and PEG·SPIONs.

3.2. Colloidal stability of PEG·SPIONs

Colloidal stability has been a key issue in biomedical applications especially under complex physiological conditions. Fig. 4A shows the colloidal stability of PEG·SPIONs at the high concentrations of sodium chloride water solutions indicated. PEG·SPIONs can be readily dispersed in NaCl solution at concentrations as high as 0.5 M. Fig. 4B shows good stability of PEG·SPIONs in a wide pH value range (pH 3–11). The corresponding PEG·SPION hydrodynamic diameters are further investigated by DLS analysis (Fig. 4C,D). The sizes appear unaffected by the conditions applied indicating excellent stability for one week. The high stability is closely associated with the hydrogen bonding between PEG and water, that renders the nanoparticles to be biocompatible, antifouling, non-immunogenic [38]. And the negatively charged surface also contributes to the colloidal stability of samples in water (Fig. 4E). These are essential properties and advantages of PEG·SPIONs especially for the *in vivo* studies.

3.3. In vitro MR relaxation of PEG·SPIONs

T_1 and T_2 of PEG·SPIONs at different Fe^{3+} concentrations in water solution were measured on a 1.41 T relaxometer at 37 °C. The r_1 and r_2 of PEG·SPIONs were determined by calculating the slope of $1/T_1$ and $1/T_2$ *versus* Fe^{3+} concentration. As shown in Fig. 5A, the r_1 and r_2 of PEG·SPIONs are 35.92 and 206.91 s^{-1} per mM of Fe^{3+} respectively. The corresponding r_2/r_1 ratio of PEG·SPIONs contrast agent is 5.76. The high r_2 as well as the low r_2/r_1 ratio make PEG·SPIONs an excellent candidate for $T_1 + T_2$ dual-contrast agent at clinically relevant magnetic field.

To further characterize PEG·SPIONs, T_1-and T_2-weighted MRI were acquired. As shown in Fig. 5B, PEG·SPIONs present bright signal enhancement in a Fe^{3+} concentration-dependent manner in the T_1-weighted MRI. In the T_2-weighted MRI, PEG·SPIONs show significant signal reduction with increasing of Fe^{3+} concentration. Similar results were also reported by Hu et al. [26].

3.4. Cytotoxicity study of PEG·SPIONs

Cytotoxicity of PEG·SPIONs was evaluated using MTT assay by incubating NIH/3T3 cells in cell culture medium containing PEG·SPIONs at

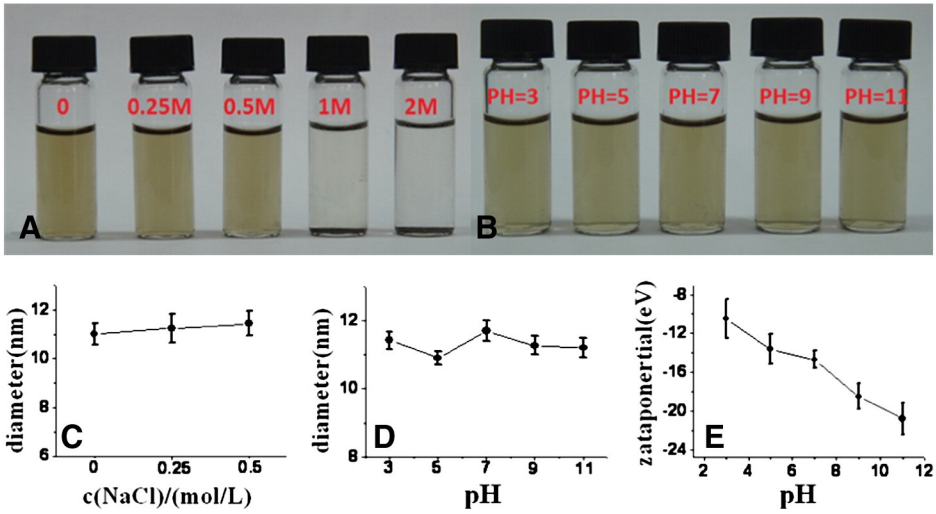

Fig. 4. Photograph of the PEG·SPIONs dispersed in various concentrations of sodium chloride water solutions (A) and with different pH buffers (B), and their corresponding hydrodynamic diameters (C, D) and the zeta potentials of PEG·SPIONs at various pH buffer solutions (E). All the samples were placed at room temperature for one week.

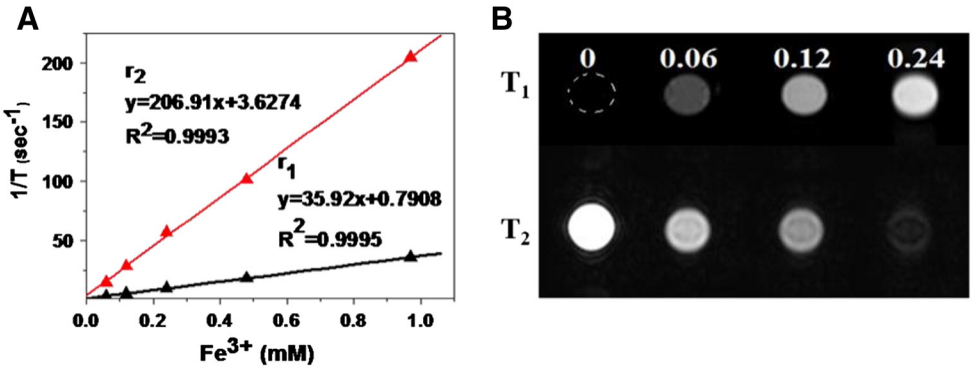

Fig. 5. The r_1 and r_2 relaxivity curves are obtained from water solutions of PEG·SPIONs with various concentrations at 37 °C (A); T_1- and T_2-weighted MR images of PEG·SPIONs with various concentrations of Fe^{3+} (from 0.06 to 0.24 mM Fe^{3+}) (B).

different concentrations (1.5 to 192 μM of Fe^{3+}) for 24 h and 48 h. The cell viability was determined by MTT assay and normalized to the control samples. The viabilities of NIH/3T3 cells are over 86% (24 h) and 67% (48 h) at the Fe^{3+} concentration of 192 μM (Fig. 6), indicating good biocompatibility of PEG·SPIONs for potential *in vivo* imaging.

3.5. In vivo MRI contrast enhancement and biodistribution of PEG·SPIONs

PEG·SPIONs were intravenously administered into Balb/c mice at the dosage of 2.5 mg Fe/kg of mouse body weight. T_2-weighted MRI was performed before and after injection. As shown in Fig. 7A, hypointensities induced by PEG·SPIONs can be readily observed in the liver and spleen at 20 min after injection. The signal-to-noise ratio (SNR) increases to ~82.6% at 20 min, and ~85.1% at 6 h in the liver. For the same time interval, the SNR increases to ~58.3% at 20 min, and ~61.3% at 6 h in the spleen (Fig. 7B). Continuous liver and spleen accumulation suggests a prolonged circulation of the nanoparticles in the bloodstream as compared to conventional MR imaging contrast agents. The contrast in the liver begins to slightly decrease after 12 h post-injection due to liver clearance. Axial liver slices of T_2-weighted MRI show intake of PEG·SPIONs and good MR contrast in various slices of the liver. *In vivo* T_1-weighted MRI post-injection of PEG·SPIONs exhibits slight signal reduction instead of enhancement (Fig. S1). Note that PEG·SPIONs show prominent $T_1 + T_2$ dual-contrast enhancement *in vitro* (Fig. 5B). Some reports on ultra small SPIONs with low r_2/r_1 value also show good T_1-enhanced MRI *in vitro*, but with few data on mice of *in vivo* MRI. This study shows that PEG·SPIONs have poor *in vivo* T_1-enhanced MRI capability, even though they show pronounced *in vitro* T_1-enhanced MRI. This would probably be related to the dispersion behaviors in the bloodstream of the injected nanoparticles.

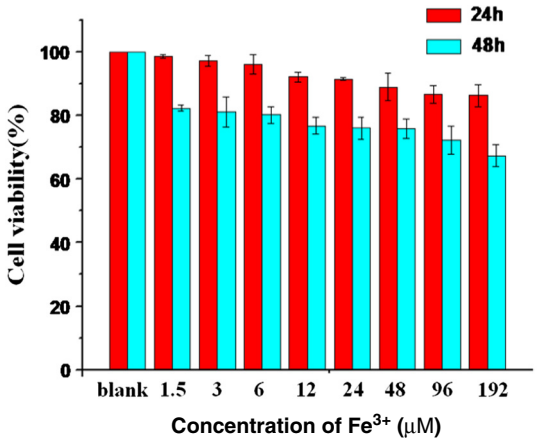

Fig. 6. Cell viability of NIH/3T3 treated with various concentrations of the PEG·SPIONs for 24 h and 48 h measured by MTT assay.

As is well known, the biodistribution profiles of nanoparticles in the body are closely related to size, composition, ligand length, and surface characteristics [39]. The surface charge of the nanoparticles greatly affects their biodistribution. Nanoparticles with neutral or zwitter ionic behavior are reported to have a reduced plasma adsorption [40,41]. In this study, PEG is dual carboxylation with negative zeta potentials (Fig. 4E). These charged PEG·SPION particles may cause plasma adsorption and the corresponding opsonization in the bloodstream. Mononuclear phagocyte system in the liver and spleen will capture these nanoparticles, which cause nanoparticles aggregated in clusters of different sizes. The nanoparticle aggregates will lead to an increase in the r_2/r_1 value, which is an adverse effect for T_1-enhanced contrast agent *in vivo*. This study suggests that the *in vitro* dispersion behaviors and imaging performance of nanoparticles are different from those *in vivo* MRI. This could be attributed to the aggregations of nanoparticles in the body. Regardless of this, the pronounced SNR change on T_2 *in vivo* indicates the high potential of PEG·SPIONs as effective T_2-weighted MRI contrast agents for tumor diagnosis.

To investigate clearance pathway and biodistribution, mice were injected with 2.5 mg/kg per body weight of PEG·SPIONs through the tail vein. At different post-injection time intervals, mice were anesthetized and sacrificed. The main organs were removed for the ICP-AES analysis of Fe^{3+} (Fig. 7C). ICP analysis shows PEG·SPIONs uptake primarily in the liver, spleen, and intestine. Much lower uptake was found in the heart, kidney or the lung. Mice injected with the nanoparticles show liver and spleen accumulations, which is consistent with the MRI images. The PEG·SPIONs are also found in the intestine at a high level for the experimental period indicated in Fig. 7C. This observation suggests an initial uptake of PEG·SPIONs by the RES system, followed by their gradual degradation and excretion *via* the hepatobiliary mechanism over a period of 14 days.

3.6. Histological analysis of animal tissues

Fig. 8 shows the histological analysis of the microscopic evaluation and the tissue-nanoparticle interactions. The *ex-vivo* experiment was performed on the tissues obtained from the harvested organs (heart, liver, spleen, lung, kidney and intestine) for any signs of toxicity. As can be seen in Fig. 8, there are no apparent histopathological abnormalities or lesions in mice compared to those of the control group. The liver, with the largest intake of PEG·SPIONs, is observed to be normal, and there are no signs of inflammatory response. Neither of any pulmonary fibrosis was detected in the lung samples. The glomerulus structure in the kidney section was microscopically distinguishable. Necrosis was not found in any of the histological samples.

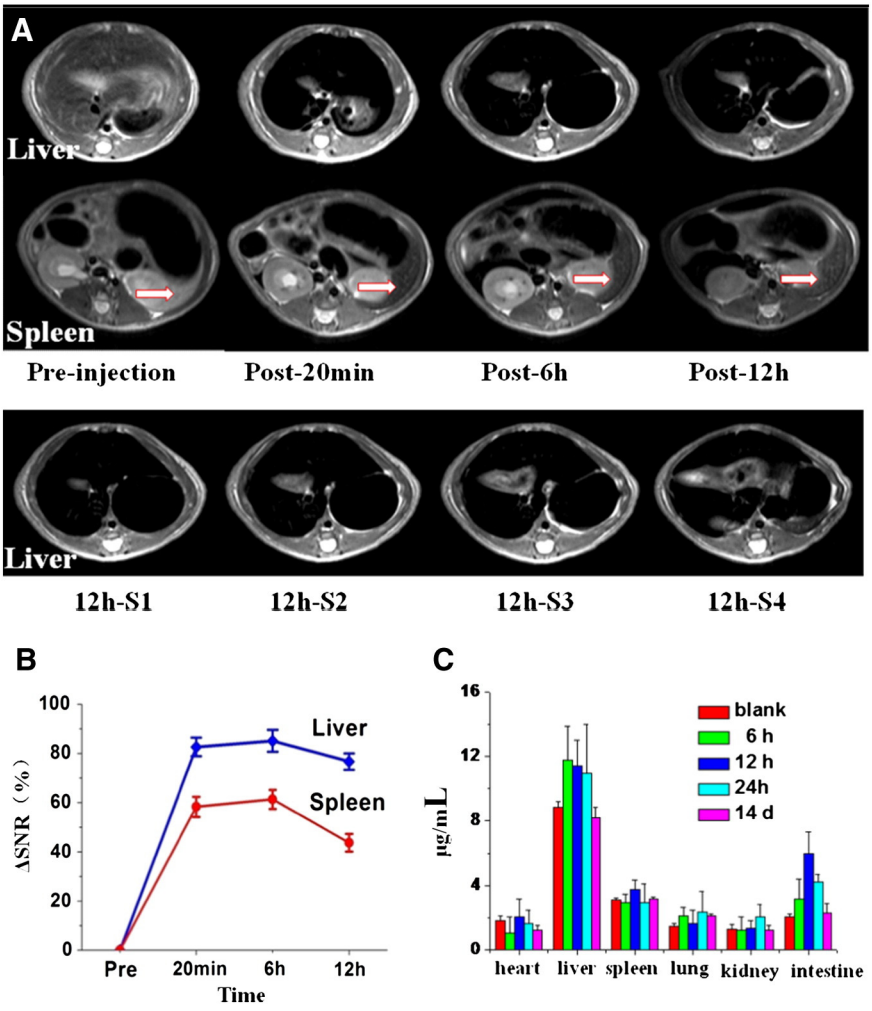

Fig. 7. MR images at the liver and spleen (the white arrow) of mice before and after tail intravenous injection of PEG·SPIONs at a dosage of 2.5 mg Fe/kg per mouse body weight (A) and relative MR signal-to-noise ratio (SNR) in the liver and spleen (B). Biodistribution in organs of mice with intravenous injection of PEG·SPIONs at different time points (C).

4. Conclusion

In conclusion, monodispersed, water-dispersible PEG·SPIONs are synthesized *via* a facile one-pot reaction. PEG·SPIONs are found colloidally stable in a wide pH range and at high ion strength. PEG·SPIONs exhibit superparamagnetic behavior, a quality that is essential to serving as the MRI contrast agent. The initial uptake of PEG·SPIONs in the liver is observed in the *in vivo* MRI experiments.

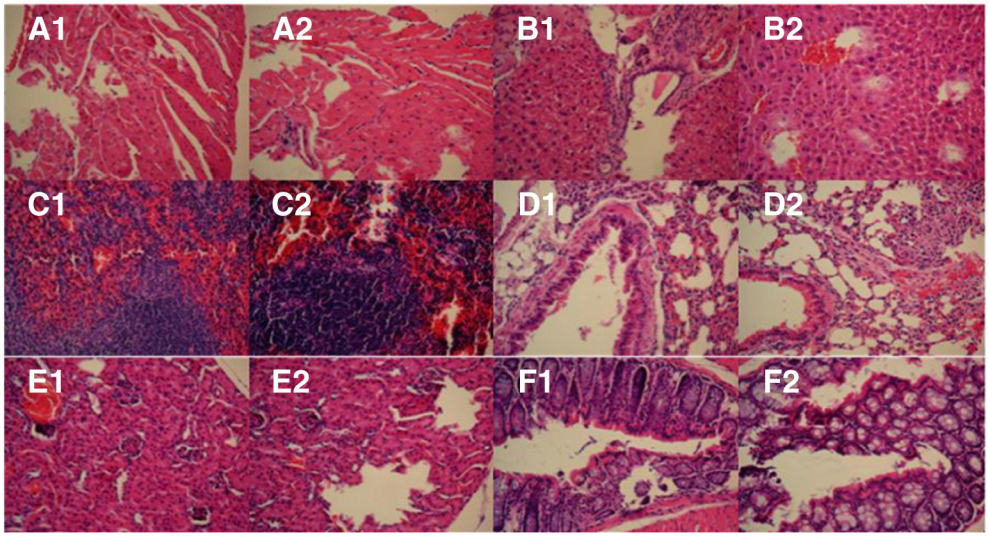

Fig. 8. Histological evaluation of the major organs: heart (A), liver (B), spleen (C), lung (D), kidney (E) and intestine (F). Hematoxylin and eosin-stained tissue sections from mice receiving no injection (A1, B1, C1, D1, E1 and F1) and injected with PEG·SPIONs 15 days post-injection (A2, B2, C2, D2, E2 and F2).

The biodistribution study shows gradual clearance of PEG·SPIONs *via* HB processing. PEG capping is found to be important for biocompatibility of PEG·SPIONs *in vitro* and *in vivo*. Based on these experimental results, the conclusion is drawn that PEG·SPIONs can be a promising candidate for the T_2-weighted MRI contrast agent.

Acknowledgments

This work was supported by the National Natural Science Foundation of China (81271630, 81371618), the "bio-medicine Innovation project" of Shanghai Science and Technology (41902502), the Shanghai Municipal Health Project (2012198), the Shanghai Innovation Program (14ZZ039), and the Nanotechnology Program of Shanghai Science & Technology Committee (11nm0504500, 12nm0500800).

Appendix A. Supplementary data

Supplementary data to this article can be found online at http://dx.doi.org/10.1016/j.msec.2014.04.041.

References

[1] S. Aime, C. Cabella, S. Colombatto, S. Geninatti Crich, E. Gianolio, F. Maggioni, J. Magn. Reson. Imaging 16 (2002) 394–406.
[2] H.R. Herschman, Science 302 (2003) 605–608.
[3] J.W. Bulte, D.L. Kraitchman, NMR Biomed. 17 (2004) 484–499.
[4] T. Schroeder, Nature 453 (2008) 345–351.
[5] H.-J. Weinmann, R.C. Brasch, W.-R. Press, G.E. Wesbey, Am. J. Roentgenol. 142 (1984) 619–624.
[6] J.G. Penfield, R.F. Reilly, Nat. Clin. Pract. Nephrol. 3 (2007) 654–668.
[7] Y.w. Jun, J.H. Lee, J. Cheon, Angew. Chem. Int. Ed. 47 (2008) 5122–5135.
[8] R. Weissleder, A. Moore, U. Mahmood, R. Bhorade, H. Benveniste, E.A. Chiocca, J.P. Basilion, Nat. Med. 6 (2000) 351–354.
[9] B. Zhang, Q. Li, P. Yin, Y. Rui, Y. Qiu, Y. Wang, D. Shi, ACS Appl. Mater. Interfaces 4 (2012) 6479–6486.
[10] S.M.C. Berman, P. Walczak, J.W.M. Bulte, Wiley Interdiscip. Rev. Nanomed. Nanobiotechnol. 3 (2011) 343–355.
[11] A. Bhirde, J. Xie, M. Swierczewska, X. Chen, Nanoscale 3 (2011) 142–153.
[12] J. Huang, L. Wang, R. Lin, Y.A. Wang, L. Yang, M. Kuang, W. Qian, H. Mao, ACS Appl. Mater. Interfaces 5 (2013) 4632–4639.
[13] C. Barrera, A.P. Herrera, N. Bezares, E. Fachini, R. Olayo-Valles, J.P. Hinestroza, C. Rinaldi, J. Colloid Interface Sci. 377 (2012) 40–50.
[14] R. Alwi, S. Telenkov, A. Mandelis, T. Leshuk, F. Gu, S. Oladepo, K. Michaelian, Biomed. Opt. Express 3 (2012) 2500–2509.
[15] V.M. Khot, A.B. Salunkhe, N.D. Thorat, R.S. Ningthoujam, S.H. Pawar, Dalton Trans. 42 (2013) 1249–1258.
[16] J.-B. Qu, H.-H. Shao, G.-L. Jing, F. Huang, Colloids Surf. B Biointerfaces 102 (2012) 37–44.
[17] M. Babic, D. Horák, M. Trchová, P. Jendelová, K. Glogarová, P. Lesný, V. Herynek, M. Hájek, E. Syková, Bioconjug. Chem. 19 (2008) 740–750.
[18] X. Wang, F. Wei, A. Liu, L. Wang, J.-C. Wang, L. Ren, W. Liu, Q. Tu, L. Li, J. Wang, Biomaterials 33 (2012) 3719–3732.
[19] S. Chen, Y. Li, C. Guo, J. Wang, J. Ma, X. Liang, L.-R. Yang, H.-Z. Liu, Langmuir 23 (2007) 12669–12676.
[20] S. Laurent, D. Forge, M. Port, A. Roch, C. Robic, L. Vander Elst, R.N. Muller, Chem. Rev. 108 (2008) 2064–2110.
[21] S. Sun, H. Zeng, D.B. Robinson, S. Raoux, P.M. Rice, S.X. Wang, G. Li, J. Am. Chem. Soc. 126 (2004) 273–279.
[22] B.L. Zhang, Z.J. Tu, F.Y. Zhao, J. Wang, Appl. Surf. Sci. 266 (2013) 375–379.
[23] L.J. Wang, Q. Wu, S. Tang, J.F. Zeng, R.R. Qiao, P. Zhao, Y. Zhang, F.Q. Hu, M.Y. Gao, RSC Adv. 3 (2013) 23454–23460.
[24] D. Vllasaliu, R. Fowler, S. Stolnik, Expert Opin. Drug Deliv. 11 (2014) 139–154.
[25] M.J. Santos-Martinez, K. Rahme, J.J. Corbalan, C. Faulkner, J.D. Holmes, L. Tajber, C. Medina, M.W. Radomski, J. Biomed. Nanotechnol. 10 (2014) 1004–1015.
[26] F. Hu, Q. Jia, Y. Li, M. Gao, Nanotechnology 22 (2011) 245604.
[27] B.H. Kim, N. Lee, H. Kim, K. An, Y.I. Park, Y. Choi, K. Shin, Y. Lee, S.G. Kwon, H.B. Na, J. Am. Chem. Soc. 133 (2011) 12624–12631.
[28] L. Sun, C. Huang, T. Gong, S. Zhou, Mater. Sci. Eng. C 30 (2010) 583–589.
[29] J. Xie, G. Liu, H.S. Eden, H. Ai, X. Chen, Acc. Chem. Res. 44 (2011) 883–892.
[30] K.G. Neoh, E.T. Kang, Soft Matter 8 (2012) 2057–2069.
[31] R. Zhu, W. Jiang, Y. Pu, K. Luo, Y. Wu, B. He, Z. Gu, J. Mater. Chem. 21 (2011) 5464–5474.
[32] K. Yoncheva, M.N. Centelles, J.M. Irache, J. Microencapsul. 25 (2008) 82–89.
[33] X. Kong, X. Li, X. Wang, T. Liu, Y. Gu, G. Guo, F. Luo, X. Zhao, Y. Wei, Z. Qian, Carbohydr. Polym. 79 (2010) 170–175.
[34] U.I. Tromsdorf, O.T. Bruns, S.C. Salmen, U. Beisiegel, H. Weller, Nano Lett. 9 (2009) 4434–4440.
[35] C. Sun, K. Du, C. Fang, N. Bhattarai, O. Veiseh, F. Kievit, Z. Stephen, D. Lee, R.G. Ellenbogen, B. Ratner, ACS Nano 4 (2010) 2402–2410.
[36] H. Otsuka, Y. Nagasaki, K. Kataoka, Adv. Drug Deliv. Rev. 64 (2012) 246–255.
[37] Q. Liu, Z. Xu, Langmuir 11 (1995) 4617–4622.
[38] L.E. van Vlerken, T.K. Vyas, M.M. Amiji, Pharm. Res. 24 (2007) 1405–1414.
[39] F. Alexis, E. Pridgen, L.K. Molnar, O.C. Farokhzad, Mol. Pharm. 5 (2008) 505–515.
[40] R. Kumar, I. Roy, T.Y. Ohulchanskky, L.A. Vathy, E.J. Bergey, M. Sajjad, P.N. Prasad, ACS Nano 4 (2010) 699–708.
[41] J. Gbadamosi, A. Hunter, S. Moghimi, FEBS Lett. 532 (2002) 338–344.